IEEE Access
Multidisciplinary ⋮ Rapid Review ⋮ Open Access Journal

Received August 11, 2020, accepted September 3, 2020, date of publication September 7, 2020,
date of current version September 21, 2020.

Digital Object Identifier 10.1109/ACCESS.2020.3022373

Manipulation of Terahertz Wave Based on Three-Layer Transmissive Pancharatnam-Berry Phase Metasurface

XUFENG JING[1,2], YOUHUANG KE[1,2], YING TIAN[1], HAIYONG GAN[3], YINGWEI HE[3], CHENXIA LI[1], AND ZHI HONG[2]

[1]Institute of Optoelectronics Technology, China Jiliang University, Hangzhou 310018, China
[2]Centre for THz Research, China Jiliang University, Hangzhou 310018, China
[3]National Institute of Metrology, Beijing 102200, China

Corresponding author: Haiyong Gan (ganhaiyong@nim.ac.cn)

This work was supported in part by the National Key Research and Development Project of China under Grant 2017YFF0206103, in part by the Natural Science Foundation of Zhejiang Province under Grant LY20F050007, and in part by the National Natural Science Foundation of China under Grant 61875159.

ABSTRACT In order to improve the transmitted efficiency of metasurfaces, the three-layer unit cell structure with coupling characteristics between layers was proposed. Using these Pancharatnam-Berry phase element particles with three-layer structure, we constructed encoded metasurfaces with different sequences to control the transmitted scattered waves. However, the manipulation of continuous transmission angle requires the continuous change of encoding metasurface period. Since the size of encoding particles in the coded metasurfaces cannot be designed to be infinitesimally small, it is impossible to obtain the continuously changing period of coded metasurfaces. In order to obtain the continuous manipulation of transmission scattering angles, we introduced the principle of Fourier convolution operation in digital signal processing on encoding metasurface sequences. By performing the addition and subtraction operation between two different encoding metasurface sequences, a new encoding metasurface sequence can be obtained with different scattering angle. The transmission scattering angles can be obtained continuously, and the terahertz wave can be manipulated freely. Moreover, by using the proposed three-layer highly efficient Pancharatnam-Berry phase encoding meta-atoms, these coded particles with different rotation angles can be precisely arranged to build the generators of the orbital angular momentum beam with different topological charges.

INDEX TERMS Metamaterial, terahertz wave, transmission.

I. INTRODUCTION

The metasurface is an artificial layered material whose thickness is less than the wavelength. Metasurface can flexibly and effectively regulate the characteristics of electromagnetic wave polarization, amplitude, phase, polarization mode and propagation mode [1]–[5]. In terms of polarization regulation, metasurface can realize polarization conversion, optical rotation, vector beam generation and other functions [6]–[8]. Metasurface can realize asymmetric light transmission, anti-reflection, enhanced transmission, magnetic mirror, EIT-like effect, etc. [9]–[11]. By controlling the phase of electromagnetic wave, the metasurface can realize the functions of beam deflection, hyperlens, hyperholography, vortex light generation, coding, stealth and illusion [12]–[14].

In general, metasurface functional devices are divided into reflection type and transmission type. At present, in order to achieve high efficiency, most of the metasurface functional devices focus on reflection mode. However, it is difficult to achieve high efficiency for transmissive metasurface functional devices due to ohmic loss and impedance mismatch. Although transmission metasurfaces exhibit unique wavefront handling, most transmission metasurfaces suffer from low efficiency. Furthermore, for transmissive metasurface functional devices to achieve phase transitions ranging from 0 to 2π, the structure of the meta-atoms units in the

The associate editor coordinating the review of this manuscript and approving it for publication was Muhammad Zubair.

metasurface requires precise control of electric resonance and magnetic resonance. Based on Huygens' principle [15], [16] or all-dielectric structure [17], a few transmissive metasurfaces have been proposed, which can show higher efficiency. However, the operation of these metasurfaces may require specific polarization added complexity in manufacturing, and the thickness of dielectric metasurfaces are comparable to the wavelength. In order to achieve the planar transmission type metasurface, the original monolayer metasurface structure was proposed, but the efficiency of this type of metasurface is only 5% [18]. Moreover, for the single-layer transmissible metasurface structure, the maximum theoretically achievable efficiency of this metasurface is only 25%, since only the electric response resonance effect can be obtained in this structure [19]. Recently, using a double split loop [20] and enclosed H-shape [21], several double-layered transmittance metasurface structures were proposed. However, most designs suffer from low efficiency.

In the applications of metasurfaces, the terahertz (THz) spectrum is of particular research interest due to its unique properties such as non-ionizing photon energy, spectral fingerprinting of inter-molecular vibrations, high transparency of certain optically opaque materials, making it highly desirable for applications in biological sensing, material analysis, and imaging [22]. However, the lack of terahertz materials and devices has seriously restricted the development of terahertz field. The main reason is that most natural materials have no electromagnetic response to terahertz waves. Recently, some Terahertz wave metasurfaces with metal and dielectric material in transmission or reflection modes have been proposed to realize various functions such as wave plate, hologram, vector beam and nonlinear harmonic generation, and so on [23]–[31]. However, these terahertz metasurfaces are mainly focused on the realization of functions and are generally inefficient. Moreover, these metasurfaces are mainly composed of resonant meta-atoms, resulting in strong dispersion characteristics of the metasurfaces. Here, we propose a three-layer transmissive metasurface structure with Pancharatnam-Berry geometric phase meta-atoms in the terahertz band. It is expected that the coupling effect between multiple layers can realize both electric resonance and magnetic resonance effects, leading to higher efficiency and phase change. Also, the phase change can be realized by simply rotating the unit structure of the Pancharatnam-Berry geometric phase meta-atoms, leading to the simplicity of design.

In order to realize the free control of the beam, we encode the designed three-layer metasurface unit cells to construct the encoded metasurface. Coding metasurface is the concept of using digital coding to describe the metasurface unit, and it can control the electromagnetic wave by changing the spatial arrangement of the coding unit [32]–[34]. Based on the generalized Snell's law and the principle of digital coding metasurface, the transmitted scattered beam can be controlled according to the particle arrangement of the coding unit. In order to obtain the continuous control of scattering angle, the periodic arrangement of the coded metasurface needs continuous changes. However, it is impossible to design infinitesimal coding unit particles, so the ordinary coded metasurface arrangement cannot realize the free control of scattering mode. In order to obtain the free control of the transmitted scattered beam, we introduce the Fourier convolution theory in digital signal processing, and carry on the addition or subtraction operation to the coded metasurface, and realize the free control of the angle of the scattered beam.

In this work, we propose to construct a high-efficiency transmission-encoded metasurface with three layers of Pancharatnam-Berry phase coding particles. Pancharatnam-Berry geometric phase electromagnetic metasurface is a kind of metasurface composed of the same artificial microstructures with different rotation angles. By simply changing the rotation angle of the microstructure unit cell, the phase mutation of the reflected (transmitted) wave can be realized, and the phase gradient or distribution can be manually controlled, thus greatly reducing the complexity of designing and machining metasurfaces. Importantly, for Pancharatnam-Berry geometric phase metasurface, we introduce Fourier convolution theory in digital signal processing to realize the addition or subtraction operation of encoded metasurfaces, so as to achieve the free control of transmission scattering pattern. Furthermore, the proposed three-layer Pancharatnam-Berry phase encoding meta-atoms can be used to construct the orbital angular momentum beam generators with different topological charges.

II. THEORY

A. PANCHARATNAM-BERRY PHASE OF ENCODING METASURFACE PARTICLES

The Pancharatnam-Berry phase can be obtained by rotating the angle of the unit structure. This convenient and flexible method of phase control is also known as geometric rotation phase. Next, we will use Jones matrix to analyze the principle of producing geometric rotational phases by using encoding metasurface particles. As shown in Fig.1, when the angle between the meta-atom unit structure and the x-axis is ρ, the scattering characteristic for this general unit cell can be

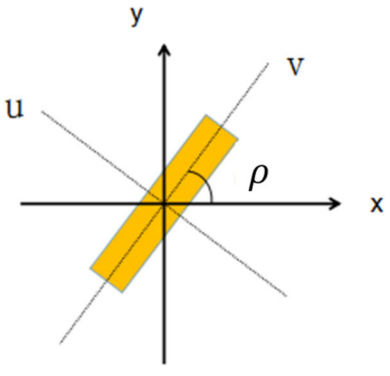

FIGURE 1. Pancharatnam-Berry geometric phase principle.

expressed by

$$T(x, y) = M[\rho(x, y)]J(\alpha)M^{-1}[\rho(x, y)] \quad (1)$$

where $J(\alpha) = \begin{bmatrix} s_1 & 0 \\ 0 & s_2 e^{i\alpha} \end{bmatrix}$, S_1 and S_2 are the scattering coefficient along the axial direction of the structure, and α is the phase delay. $M(\rho) = \begin{bmatrix} \cos\rho & \sin\rho \\ -\sin\rho & \cos\rho \end{bmatrix}$ is rotation matrix. When $|R\rangle = (1, 0)^T$ is a right-hand circularly polarized light, and $|L\rangle = (1, 0)^T$ is a left-hand circularly polarized light, the emitting light field can be expressed as

$$|E_{out}\rangle = h_E |E_{in}\rangle + h_R exp[i2\rho(x, y)] |R\rangle + h_L exp[-i2\rho(x, y)] |L\rangle \quad (2)$$

where

$$\eta_E = \frac{1}{2}[e_1 + e_2 \exp(i\alpha)],$$
$$\eta_R = \frac{1}{2}[e_1 - e_2 \exp(i\alpha)]\langle E_{in} |L\rangle,$$
$$\eta_L = \frac{1}{2}[e_1 - e_2 \exp(i\alpha)]\langle E_{\text{in}} |R\rangle,$$

$\langle E_{in} \mid R\rangle$ indicates coupling efficiency, e_1 represents the amplitude of the electric field perpendicular to the direction of the metal strip, and e_2 represents the amplitude of the electric field parallel to the direction of the metal strip in Fig.1. Therefore, it can be obtained that the emitted light field contains circularly polarized light with geometric phases. If the rotation angle from 0° to 180° can be implemented, the transmitted light wave can be obtained with phase changes from 0° to 360°.

B. FAR FIELD SCATTERING PRINCIPLE OF CODED METASURFACES

Figure 2 shows the far field scattering diagram of 1-bit coded metasurface in transmission mode. The yellow block and the black block represent the "0" and "1" digital encoding units, which correspond to the phase changes of 0 and π, respectively. And d_x and d_y respectively represent the length of each coding unit in the x and y directions, and they are scalars. Γ_x and Γ_y respectively refer to the super period of encoding metasurface in the x and y directions. The coded metasurface consists of an M × N square grid. Based on the traditional phased array antenna theory [35], when a plane wave is incident on the coded metasurface, the far-field scattering can be expressed as

$$F(\theta, \varphi) = \sum_{m=1}^{M} \sum_{n=1}^{N} T_{m,n} e^{-i(kd_x(m-\frac{1}{2})\sin\theta\cos\phi + kd_y(n-\frac{1}{2})\sin\theta\sin\phi)} \quad (3)$$

where k is the wave number, $T_{m,n}$ denotes the transmission coefficient of unit structure (m, n), and θ and φ is the elevation angle and azimuth angle of scattering. For 1-bit coding metasurface, the transmission coefficient of coding unit is assumed to be approximately 1, and the phase difference of each coding unit is 0 or π, and $\varphi_0 = 0$. Eq.(3) can be further simplified as

$$F(\theta, \varphi) \sum_{m=1}^{M} e^{-i(kd_x(m-\frac{1}{2})\sin\theta\cos\phi + m\pi)} \sum_{n=1}^{N} e^{-i(kd_y(n-\frac{1}{2})\sin\theta\sin\phi + n\pi)} \quad (4)$$

Thus, the far-field scattering strength can be expressed as

$$|F(\theta, \phi)| = MN \sin c(m\pi)(p + \frac{1}{2} - \frac{m}{2}kd_x \sin\theta\cos\phi) \sin c(n\pi(q + \frac{1}{2}) - \frac{n}{2}kd_y \sin\theta \sin\phi \quad (5)$$

where p, q = 0, ±1, ±2 . . .. It can be obtained from Eq. (5) that $|F(\theta, \varphi)|$ reaches its first extreme value, when it satisfy the following conditions as

$$\phi = \pm\tan^{-1}\frac{d_x}{d_y}, \quad \phi = \pi \pm \tan^{-1}\frac{d_x}{d_y}, \quad (6)$$

$$\theta = \sin^{-1}\left(\frac{\pi}{k}\sqrt{\frac{1}{d_x^2} + \frac{1}{d_y^2}}\right) \quad (7)$$

When $\Gamma_x = 2d_x$, $\Gamma_y = 2d_y$, and $k = 2\pi/\lambda$, Eq.(7) can be simplified as

$$\theta = \sin^{-1}\left(\lambda\sqrt{\frac{1}{\Gamma_x^2} + \frac{1}{\Gamma_y^2}}\right) \quad (8)$$

For the encoding metasurface, where the phase gradient changes along one direction, such as $\Gamma_x \to \infty$, or $\Gamma_y \to \infty$, Eq.(8) for the elevation angle θ of the anomalous beam can be simplified as

$$\theta = \sin^{-1}\left(\frac{\lambda}{\Gamma}\right) \quad (9)$$

It should be noted that these functions also can be applicative for coding metasurface with multiple bits or the reflection coding metasurface.

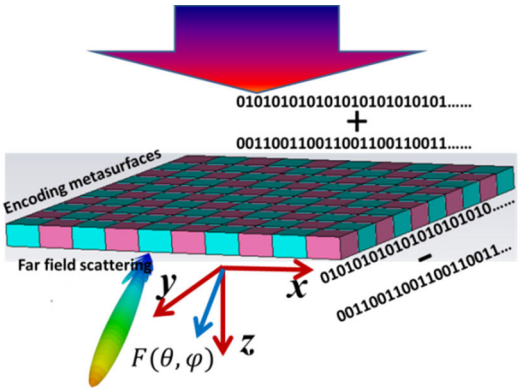

FIGURE 2. Conceptual illustration of the transmission-type coding metasurface to refract the normal incidence in anomalous direction. Far-field scattering diagram of coded metasurface in transmission mode.

C. CONVOLUTION OPERATION PRINCIPLE OF ENCODING METASURFACES

In digital signal processing system, the time domain signal and frequency domain signal are Fourier transform pair. One can convert the product of two signals in the time domain into the convolution of two signals in the frequency domain, and then invert it. So, this calculation can be expressed as

$$f(t) \cdot g(t) \overset{FFT}{\Leftrightarrow} f(w) * g(w) \tag{10}$$

Similarly, the near-field distribution and far-field scattering pattern of the coded metasurface sequences are also Fourier transform pairs. Thus, an encoding metasurface sequence can be equivalent to the time domain signal as $t \rightarrow x_\lambda = T/\lambda$, where x_λ is electric length. The far field scattering pattern of encoding metasurface can be equivalent to the frequency domain signal as $\omega \rightarrow sin\theta$, where θ is scattering angle. The time signal t and frequency signal ω in digital signal processing can be similarly replaced by the coding sequence and the far-field scattering mode respectively as

$$f(x_\lambda) \cdot g(x_\lambda) \overset{FFT}{\Leftrightarrow} f(\sin\theta) * g(\sin\theta) \tag{11}$$

When $g(\omega)$ is the Dirac function, Eq.(10) can be further derived as

$$f(t) \cdot e^{i\omega_0 t} \overset{FFT}{\Leftrightarrow} f(\omega) * \delta(\omega - \omega_0) \tag{12}$$

Similarly, Eq.(11) can be further deduced as

$$f(x_\lambda) \cdot e^{i \sin\theta_0 x\lambda} \overset{FFT}{\Leftrightarrow} F(\sin\theta - \sin\theta_0) = F(\sin\theta - \sin\theta_0), \tag{13}$$

where $e^{i \sin\theta_0 x_\lambda}$ represents a coded sequence with unit amplitude and gradient phase. The left-hand side of Eq.(13) represents the addition operation of two coded hypersurface sequences, and the right-hand side of the formula represents the addition operation of the corresponding scattering mode. The new encoding sequence $f(x_\lambda) \cdot e^{isin\theta_0 x_\lambda}$ can be obtained by adding the original encoding sequence $f(x_\lambda)$ to a gradient phase encoding sequence $e^{isin\theta_0 x_\lambda}$. At the same time, we can obtain a new encoding sequence $f(x_\lambda) \cdot e^{-isin\theta_0 x_\lambda}$ by subtracting a gradient phase coded metasurface sequence $e^{isin\theta_0 x_\lambda}$ from the original encoding sequence $f(x_\lambda)$. The negative sign in the coding sequence $e^{-isin\theta_0 x_\lambda}$ indicates that it is the opposite of the coding sequence $e^{isin\theta_0 x_\lambda}$. It should be noted that the scattering angles of the new encoding sequence after Fourier convolution operation cannot be obtained by adding or subtracting the scattering angles of the two encoding sequences. The scattering angle of the new coded sequence should be calculated by $\theta' = sin^{-1}(sin\theta_1 \pm sin\theta_2)$, where θ_1 and θ_2 represent the scattering angles of the two coded metasurface sequences, respectively, and $sin\theta_1 + sin\theta_2 < 1$.

III. DESIGN OF ENCODING METASURFACE

Firstly, we need to design the unit structure encoding particles that encode the metasurface. It is known that both the magnetic and electric resonances should be precisely controlled for the transmissive metasurfaces. For a single layer metasurface structure, the low efficiency can be predicted due to only electric response realized in such structures. Both electric and magnetic resonances can be achieved in a multilayer system. The magnetic response can be achieved by interlayer coupling effect. The presence of both electric and magnetic responses provides more freedom to tune the transmission characteristics of meta-atoms. Also, the crucial role of magnetic response is to achieve the impedance matching, resulting in high efficiency of designed devices. Considering the difficulty of preparing a metasurface, we hope to design metasurface unit structure with as few layers as possible. The metasurface structures with more layers are more difficult to prepare. However, several double-layered transmittance metasurface structures suffer from low efficiency [20], [21]. So, we propose a three-layer meta-atom unit structure, which is expected that high efficiency can be achieved.

After precise optimization and design, we obtained the transmission-based coding metasurface coding particle structure as shown in Fig.3. The top double bar metal structure and its lower medium layer are regarded as one layer, and the middle metal structure is considered as one layer. The lower medium and double bar metal, which are symmetric with the uppermost structure, are regarded as the third layer. For the unit cell of encoding metasurface in Fig.3, the two metal bars in each layer have exactly the same structure and are arranged symmetrically. The copper material is used for metal structure with the thickness of 100nm. The dielectric layer uses polyimide material with the permittivity of 3.5. In Fig.3(c)(d), a = 84 μm, w1 = 7μm, w2 = 18μm, L = 100μm, d = 88μm, and h = 30μm.

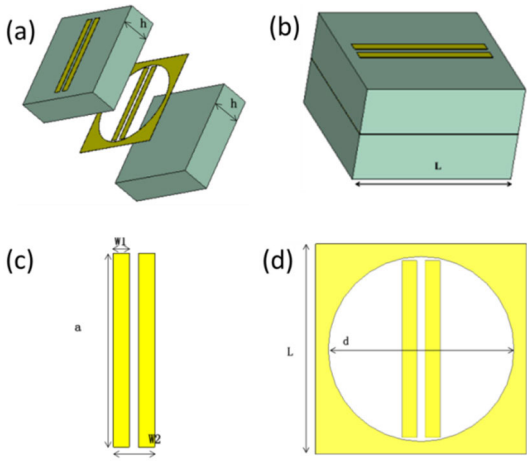

FIGURE 3. Schematic diagrams of designed meta-atom encoding unit cell. (a) Separated three-layer structure. As the metal layer is relatively thin, the first metal layer and the lower medium layer are regarded as one layer, and the bottom metal layer and the medium layer are regarded as one layer. The metal structure of the third layer is located below the medium layer. The middle metal layer is a key layer, and the middle metal layer is regarded as one layer. The whole meta-atom unit structure can be regarded as a three-layer structure. (b) Schematic diagram of three-layer unit structure designed. (c) Schematic diagram of the metal structure of the first and third layers. The metal structure of the first layer is the same size as the metal structure of the third layer. (d) Schematic diagram of the intermediate metal layer.

When a beam of light is incident on the metasurface, there will be four beams, normal reflection, abnormal reflection, normal transmission and abnormal transmission as

$$\begin{cases} T_n \equiv \left|t_{xx} + t_{yy}\right|^2/4 \\ R_n \equiv \left|r_{xx} + r_{yy}\right|^2/4 \\ T_a \equiv \left|t_{xx} + t_{yy}\right|^2/4 \\ R_a \equiv \left|r_{xx} - t_{yy}\right|^2/4 \end{cases} \tag{14}$$

In order to obtain high efficiency abnormal transmission, other beams should be suppressed. Based on Eq. (14), it can be seen that if the metasurface element structure meets the following conditions, higher abnormal transmission efficiency can be obtained as

$$\begin{aligned} r_{xx} &= r_{yy} = 0, \\ |t_{xx}| &= \left|t_{yy}\right| = 1, \\ \arg(t_{xx}) &= \arg(t_{yy}) \pm \pi \end{aligned} \tag{15}$$

By using the finite integral method, we obtain the initial unit structure of the coded metasurface after optimization design. The amplitude and phase of transmission are shown in Fig.4. It can be seen that the higher transmission above 0.89 can be achieved, and the phase difference of π can be obtained for the two cross polarization incidence at 0.737THz. These amplitude and phase conditions basically satisfy Eq.(5), and the Pancharatnam-Berry phase encoding particles can be obtained by rotating this designed unit structure when the circularly polarized wave is incident.

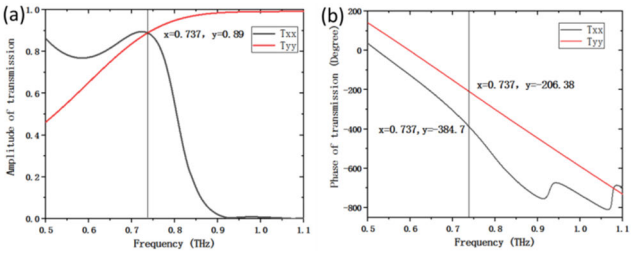

FIGURE 4. (a) The co-polarized transmission magnitude, (b) The co-polarized transmission phase shift.

Next, we will construct four 2-bit coded particles by rotating the unit structure as shown in Table 1. When $\alpha = 0°$, $\alpha = 45°$, $\alpha = 90°$, and $\alpha = 135°$ in Table 1, we can define respectively them as encoding particles "0", "1", "2", "3". The phase variations of the four coded particles for the cross-polarized wave are shown in Fig.5 when the left-handed circularly polarization wave is incident. It can be seen that at 0.737THz a phase change of nearly 90 degrees can be obtained between the four coded particles. Thus, these four coded particles can accurately construct 2-bit coded metasurfaces by rotating at different angles.

IV. FOURIER CONVOLUTION OPERATION OF ENCODING METASURFACE SEQUENCES

Next, we will construct three basic coding metarsurface sequences by using four coding particles as

TABLE 1. Four 2-bit encoding particles.

Encoding particles	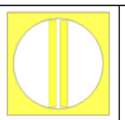		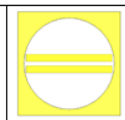	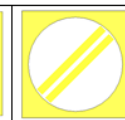
α	0°	45°	90°	135°
Digital coding	"0"	"1"	"2"	"3"

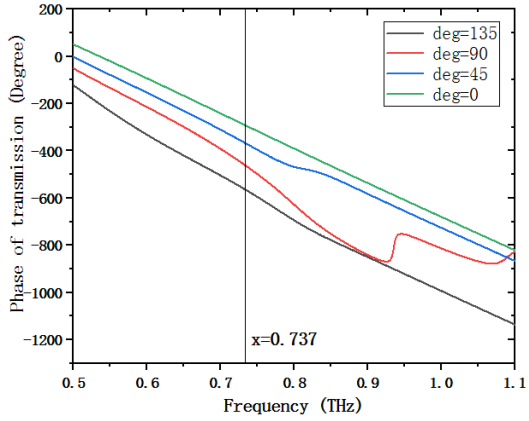

FIGURE 5. The phase variation of the four coded particles with the different rotation angle of the initial structure.

S1(00112233.....), S2(000111222333.....) and S3(0000111122223333.....). Figure 6(a) show respectively the schematic diagram of three basic sequence coding metaurfaces. The corresponding scattering angle for the cross-polarization wave is shown in Fig.6(b) and Fig.6(c) when the left-handed circularly polarization wave is incident. It can be seen that the transmitted scattering angles of 27°, 19°, and 14° for the encoding sequences S1, S2, and S3, respectively, can be obtained by numerically simulation. For the encoding metasurfaces S1, S2, and S3, the phase gradient changes are along x-direction with $\Gamma_y \to \infty$. For S1, S2, and S3, the corresponding super-periods of encoding metasurfaces are of $T_x = 8\text{L}$, $T_x = 12\text{L}$ and $T_x = 16\text{L}$, respectively, with $\text{L} = 100\mu m$. Based on Eq.(9), the scattering angles can be calculated theoretically as

$$\begin{aligned} \theta_{S1} &= arcsin\frac{\lambda}{T_x} = arcsin\frac{300 \div 0.737}{8 \times 100} = 30.59 \\ \theta_{S2} &= arcsin\frac{\lambda}{T_x} = arcsin\frac{300 \div 0.737}{12 \times 100} = 19.83 \\ \theta_{S2} &= arcsin\frac{\lambda}{T_x} = arcsin\frac{300 \div 0.737}{16 \times 100} = 14.73. \end{aligned}$$

After calculation, the transmitted scattering angles of 30.59°, 19.83°, and 14.73° for the encoding sequences S1, S2, and S3, respectively, can be obtained. The numerical simulation results are in agreement well with that of theoretically calculations. Equation 9 presents a relation between super period and scattering angle at a fixed wavelength. In designed sequences S1, S2, and S3, each element is repeated two, three

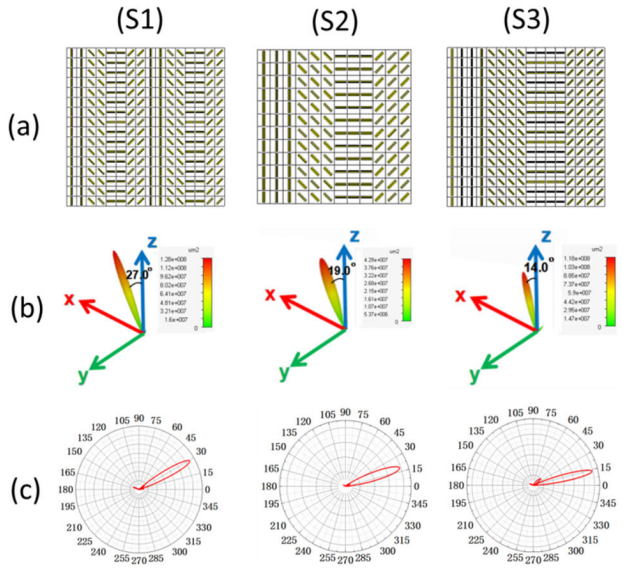

FIGURE 6. (a) Encoding metasurface sequences S1, S2, and S3, (b) transmitted three-dimension scattering for three encoding metasurface sequences, respectively. (c) The corresponding two dimensional angle of scattering.

and four times adding another periodicity. If we use the PB cell structure to design the coding sequences as S1, S2 and S3 with the same period and without the repetitions of unit cells, the far field scattering angle of the coded metasurface sequences does not change according to Eq.(9). However, the scattering efficiency may be improved because of the momentum matches between the particles.

Based on the generalized Snell's law and far field scattering characteristics of encoding metasurface, the scattering angle mainly depends on the period of the coded metasurface. However, the period of the coded metasurface cannot change continuously due to the size limitations of the coded particles. If one wants the transmission scattering angle to be freely controlled, one needs to use the addition and subtraction operation of the coded metasurface sequences. Analogous to the Fourier convolution operation in digital signal processing, the coded metasurface sequences can be added or subtracted to obtain a new coded metasurface sequence, realizing the free control of scattering angle. For example, for the basic gradient encoding sequences S1(00112233……), S2(000111222333……) and S3(0000111122223333……), the four-bit operation can be performed based on these basic sequences and Fourier convolution principle, such as $0+0=0, 0+3=3, 2+2=0, 3+2=1, 3+3=2$, and so on. Also, the four-bit operation can be used to the subtraction manipulation of Fourier convolution principle for two encoding sequences. So, the new encoding sequences S4 and S5 can be obtained as $S4 = S1 - S3 = 3300001111222233\ldots\ldots$ and $S5 = S1 + S3 = 0011220022331122\ldots\ldots..$, respectively. The addition and subtraction operations for the two basic coding sequences S1 and S3 are shown in Fig.7. Two new coded metasurface sequences of S4 and S5 can be obtained.

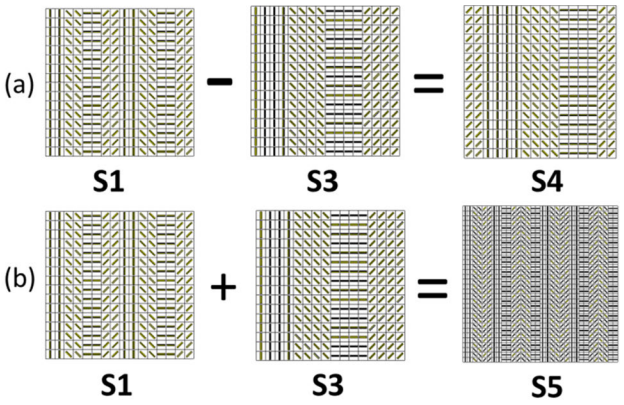

FIGURE 7. (a) Subtraction operation for two basic coding sequences S1 and S3, a new sequence S4 is obtained. (b) Addition operation for two basic coding sequences S1 and S3, a new sequence S5 is obtained.

For the new encoding metasurface sequences of S4 and S5, the scattering pattern is indicated in Fig.8. The transmitted scattering angles of 14° and49° can be obtained by numerically simulation for the encoding metasurface sequences S4 and S5, respectively. According to Fourier convolution principle of encoding metasurfaces in Eq.(13), the theoretically scattering angles can be calculated as 14.74° and 49.74° for the encoding sequences S4 and S5, respectively. It can be seen that the numerical results are in good agreement with the theoretical results. The addition and subtraction principles of coded metasurface sequences are further proved.

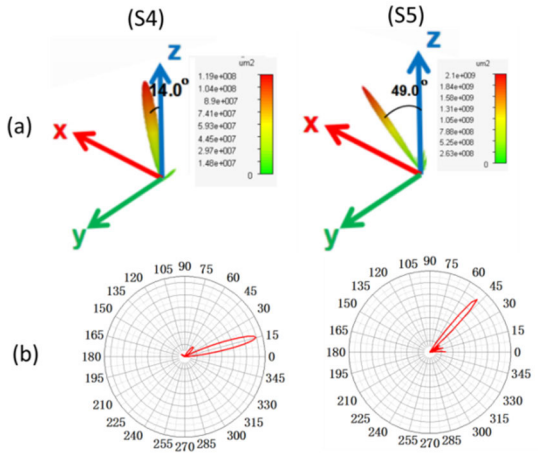

FIGURE 8. (a) 3D scattering pattern for S4 and S5, respectively, (b) The corresponding 2D scattering angle for S4 and S5, respectively.

Moreover, the addition and subtraction operation for two basic coding sequences S1 and S2 can be implemented, and the two new encoding metasurface sequences S6 and S7 can be obtained in Fig.9. $S6 = S1 + S2 = 00123311230022301133012 2$, and $S7 = S1 - S2 = 33030000101111212222323 3$. Four-bit Fourier convolution operation of S1 and S2 is verified to obtain a different deflection angle under the left-handed circularly polarization wave as shown in Fig.9. Figure 9(b) and Fig.9(c) show the

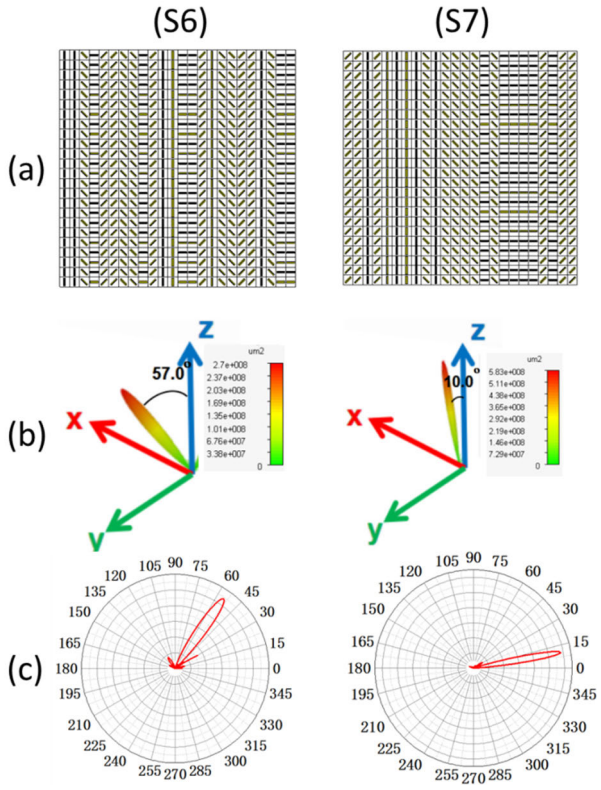

FIGURE 9. (a) Encoding metasurface sequences for S6 and S7, respectively. (b) The corresponding 3D transmitted scattering pattern. (c) 2D scattering pattern.

far-field scattering patterns of S6 and S7. The abnormal deflection angles of the encoding sequences S6 and S7 are 57° and 10°, respectively, which is basically consistent with the theoretical results of 58° and 9.76°. Fourier convolution addition and subtraction for different basic coding sequences (S1, S2, and S3) can be performed. Next, we will add and subtract the coded metasurfaces of non-basic sequences. For the non-basic encoding sequences S6 and S7, the addition operation can be made as S8 = S6 + S7 = 33113311 ..... However, the sine of theoretical scattering angle is larger than 1 according to Eq.(9). As shown in Fig.10, some energy is emitted along the horizontal plane. The subtraction calculation of the Fourier convolution principle for S6 and S7 can be performed as S9 = S6 − S7 = 333111333111. Figure 11 shows the new encoding sequence S9 and the corresponding scattering pattern. The theoretical scattering angle is 42.72°, which is in good agreement with that of numerical simulation.

To further demonstrate that Fourier convolution can be applied to general checkerboard coding sequences, we will give the addition operation of checkerboard encoding and phase gradient encoding sequence S1. The chessboard coding pattern can be expressed by matrix M as $M = \begin{pmatrix} 0 & 2 \\ 2 & 0 \end{pmatrix}$, where each digit consist of 3*3 identical encoding particles. The whole chessboard encoding metasurface is shown

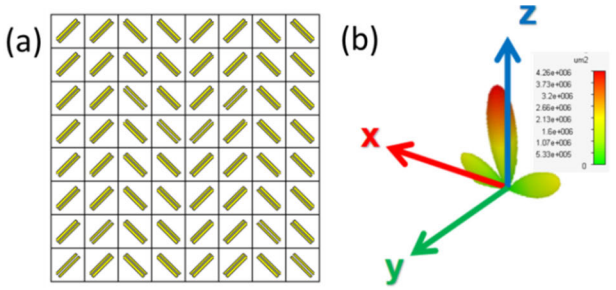

FIGURE 10. (a) The new encoding metasurface sequence S8, (b) the corresponding scattering pattern.

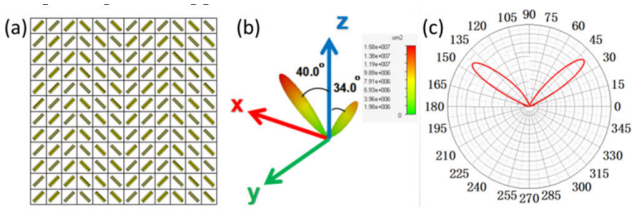

FIGURE 11. (a) Encoding metasurface sequence S9, (b) the corresponding scattering pattern, (c) 2D scattering pattern.

in Fig.12(a). Four beams with equal angle of θ with respect to the z-direction are indicated in far-field scattering pattern. Next, we introduce a gradient coding sequence *S1* (00112233……) along the horizontal direction as shown in Fig.12(b). After addition operation between the chessboard encoding metasurface and S1, the new chessboard encoding metasurface sequence can be obtained in Fig.12(c). The corresponding transmitted scattering pattern is shown in Fig.12(c), and it can be seen that the whole pattern is tilted away from the z-direction.

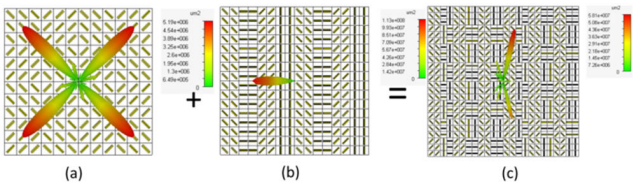

FIGURE 12. Fourier convolution operation of addition for checkerboard encoding metasurface sequences, (a) the checkerboard encoding metasurface sequence, (b) Phase gradient variation encoding metasurface sequence S1, (c) the new checkerboard encoding metasurface sequence.

V. VORTEX BEAM GENERATION OF ENCODIN METASURFACES

Orbital angular momentum (OAM) beam carries the orbital angular momentum with a helical phase, and the light field expression contains the phase factor $e^{-jl\phi}$ associated with azimuth angle ϕ and integer topological charges l. Because of its unique properties, the orbital angular momentum beam has a wide range of applications in micro-manipulation [36], [37], communication [38], [39], biomedicine [40] and information storage [41], [42], and many other fields [43]–[45]. Here,

we designed an encoding metasurface phase plate consisting of an array of 20*20 scatters that constructed by dividing the whole surface into eight consecutive segments. The phase increments between two adjacent segments are $\pi/4$ for OAM mode $l = 1$ in Fig.13(a). Figure 13(b) shows corresponding far-field scattering intensity distribution of the whole vortex beam. The corresponding phase distribution of transmission is indicated in Fig.13(c). The broadband far-field scattering characteristics of vortex beam generator with $l = 1$ from 0.6THz to 1.0THz is demonstrated in Fig.14. The phase increments between two adjacent segments are $\pi/2$ for the topological charge number $l = 2$ as shown in Fig.15. It can be seen that the OAM beam patterns are very obvious in the magnitude and phase profiles. In Fig.15(b), the null point in the center of the electric magnitude distribution is demonstrated, and the phase rotation from 0 to 4π in Fig.15(c) is disclosed for $l = 2$. The broadband far-field scattering characteristics of vortex beam generator with $l = 2$ from 0.68THz to 0.88THz is demonstrated in Fig.16.

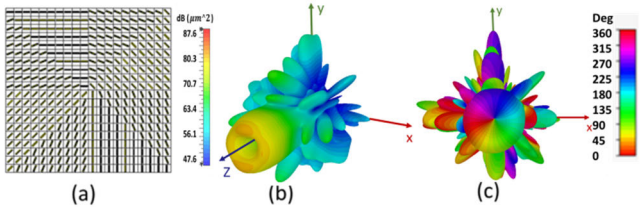

FIGURE 13. (a) Phase plate design based on coded metasurface for $l = 1$ at 0.74THz, (b) corresponding far-field scattering intensity distribution, (c) phase profile.

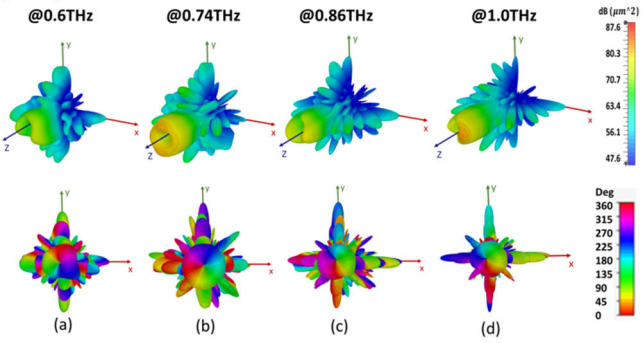

FIGURE 14. The broadband far-field scattering characteristics of vortex beam generator with $l = 1$, (a) at 0.6THz, (b) at 0.74THz, (c) at 0.86THz, (d) at 1.0THz.

Table 2 demonstrates the comparison of the proposed orbital angular momentum beam generator by using three-layer Pancharatnam-Berry phase coding meta-atoms with previous works in terms of the structure, the number of layer, the thickness, the bandwidth, the polarization and the efficiency. Compared with previously proposed generators of OAM [46]–[57], the significant advantages of our proposed OAM generator are the potential simplicity of design and preparation and its high efficiency in wide

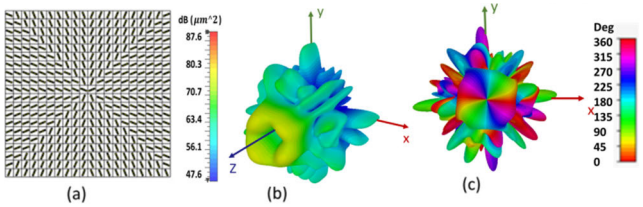

FIGURE 15. (a) Phase plate design based on coded metasurface for $l = 2$ at 0.74THz, (b) corresponding far-field scattering intensity distribution, (c) phase profile.

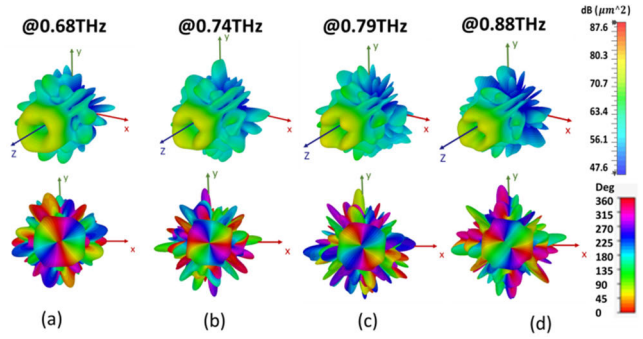

FIGURE 16. The broadband far-field scattering characteristics of vortex beam generator with $l = 2$, (a) at 0.68THz, (b) at 0.74THz, (c) at 0.79THz, (d) at 0.88THz.

bandwidth. Most of the previous designs of OMA generators used the resonance type of meta-atoms structure, and the delicate and time-consuming design is required by using the change of the element structure parameters. In our design, the three-layer highly efficient Pancharatnam-Berry phase encoding metasurface particles are proposed, and the phase control can be realized by rotating simply the unit structure angle. We arranged these coded particles with different rotation angles to construct the orbital angular momentum beam generator with different topological charges. Also, our proposed OAM generator has a broad band effect with Pancharatnam-Berry phase encoding meta-atoms, which overcomes the intrinsic dispersion of the conventional OAM generators.

Thus, we have proposed the three-layer high efficiency transmissive Pancharatnam-Berry phase metasurface to freely manipulate the scattering angle of terahertz waves. Also, the orbital angular momentum beam with different topological charges can be generated by using our designed metasurfaces. In fact, the transmissible metasurfaces may be more useful in practical applications than the reflective metasurfaces. Transmission efficiency is a key parameter of transmissible metasurface devices. However, the realization of high efficiency for the transmissive Pancharatnam-Berry phase metasurface devices is difficult, especially in ultrathin metasurfaces. Recently, a single layer transmissive Pancharatnam-Berry phase metasurface was proposed, and the maximum achievable efficiency was theoretically predicted to be 25% due to only electric responses [19], [58], [59]. For the transmissive

TABLE 2. Comparison of the proposed vortex beam generator with other works.

References	Unit cell size	Number of layers	Thickness	Bandwidth	Polarization	Transmission/ Reflection	Efficiency[10]
[46]	0.65λ	One	0.14λ	16.9%	LP	Reflection	64%
[47]	0.32λ	Four	0.72λ	33.3%	CP	Transmission	60%
[48]	0.49λ	One	0.05λ	71%	CP	Transmission &Reflection	20%
[49]	0.77λ	One	0.23λ	43.4%	LP	Reflection	65%
[50]	0.43λ	Four	0.66λ	25%	CP	Transmission	82.1%
[51]	1.1λ	One	0.01λ	90%	CP	Transmission	NA
[52]	0.27λ	One	1.3λ	0.8THz	CP	Transmission	22%
[53]	0.23λ	Three	0.07λ	28.5%	LP	Transmission	NA
[54]	0.98λ	One	1.3λ	0.78THz	LP	Transmission	NA
[55]	0.33λ	One	0.03λ	0.33THz	LP&CP	Transmission	NA
[56]	0.42λ	One	0.37λ	6.6%	LP	Reflection	90%
[57]	0.61λ	One	1.5λ	37.7%	CP	Transmission	55%
This work	0.27λ	Three	0.16λ	50%	CP	Transmission	89%

Pancharatnam-Berry phase metasurfaces, both the electric and magnetic resonant responses should be precisely controlled to achieve high efficiency and phase change covering 2π. The bilayer transmissive Pancharatnam-Berry phase metasurfaces with the double split loop or enclosed H-shape were proposed [30]. The periodic unit cell transmittance for designed metasurfaces can be achieved to be about 70%. Moreover, a bilayer transmissive Pancharatnam-Berry phase metasurface with the complementary split ring resonators was proposed, but the maximum of 55% conversion efficiency to generate the orbital angular momentum beam was observed [60]. In our work, we proposed the transmissive three layer Pancharatnam-Berry phase metasurface to realize high efficiency of near 80%. Compared with those reported transmissive Pancharatnam-Berry phase metasurfaces, the transmission efficiency of devices with the three layer structure in our work can be enhanced. By using transmissive Pancharatnam-Berry phase metasurfaces, a variety of functional devices can be implemented such as the photonic spin Hall effect, the beam deflection, the holographic imaging and so on [61]. Importantly, our designed high efficient three-layer transmitted Pancharatnam-Berry phase metasurface can be used to realize freely control of terahertz beam scattering angle by using the Fourier convolution principle.

Although the results of numerical simulation are presented in this paper, the preparation of the three-layer high-efficiency transmissible metasurfaces proposed by us can also be realized [10]. The preparation process mainly includes the traditional photolithography and the preparation of metal films. Firstly, a thick metal layer can be manufactured by using the electron beam evaporation method on silicon wafer. Then, a polyimide layer is spun onto the metal layer and baked on a hot plate. The spinning and baking processes can be repeated twice to produce a thicker polyimide layer. Next, the standard lithography processes can be implemented. The final single metal structure can be obtained through a liftoff process. Finally, the metal pattern and polyimide layers can be separated from the silicon substrate, and the monolayer metasurface structures can be obtained. The above process can be repeated to obtain the other two layers of metasurface structures. The experimental bonding method can be used to obtain the three-layer transmissible metasurface structure.

In order to measure the scattering characteristics of the prepared samples, the far-field in-plane scanning measurement with a rotary terahertz time domain system (THz-TDS) can be performed. The fiber-based terahertz photoconductive antennas can be used to generate and receive the terahertz signals in time domain. The optical stabilization platform and the rotary stage should be used for the transmitter and the receiver. In the measurement, the receiver can be rotated in the horizontal plane to record the electric fields scattered from the samples.

It should be noted that all dielectric metasurface structures have been proposed in our previous paper [62], and the element structure of the proposed metasurface belongs to resonant type of metasurfaces [63], [64]. This kind of resonance phase metasurface can move the resonance frequency through the change of structural parameters, and then change the phase of a certain frequency point, resulting in phase mutation. However, this resonance type metasurface has some problems. Because the phase mutation comes from the structural resonance, this leads to the limited working bandwidth of the resonance phase metasurface. At the same time, it also requires precise design and processing of structural dimensions with small differences to accurately control the phase. Moreover, the thickness of all-dielectric metasurface structure we have proposed before is relatively large, which causes the difficulties in preparation in the terahertz band. Here, in order to solve these problems, we propose a transmissive three-layer Pancharatnam-Berry phase metasurface. This geometric Pancharatnam-Berry phase electromagnetic metasurface is composed of the same artificial microstructure with different rotation angles. It can realize the phase mutation of the transmitted wave by simply changing

the rotation angle of the microstructure, thereby realizing manual control of the phase gradient or distribution. This kind of Pancharatnam-Berry phase metasurface can greatly reduce the complexity of design and fabrication. The emergence of this geometric phase electromagnetic metasurface gives us more freedom to manipulate electromagnetic waves. More importantly, the unit particles of this transmissive Pancharatnam-Berry phase microstructure can be precisely encoded to construct the encoding metasurface. By using Fourier convolution principle in digital signal processing, the addition and subtraction operations on the high efficient transmissive Pancharatnam-Berry phase metasurfaces with different sequences can be implemented to obtain a new coding sequence and realize freely manipulation of terahertz waves.

VI. CONCLUSION

We propose a three-layer PB phase metasurface structure, and the transmission efficiency is significantly higher than that of single-layer and double-layer structures. In the terahertz band, we encode the proposed unit particles to construct the coded metasurface with different encoding sequences. In order to realize the free control of the transmission scattering angle of the coded metasurface, we introduce the Fourier convolution principle and perform 4-bit addition and subtraction operations on different coded metasurface sequences to obtain new coded sequences. In addition, the proposed PB phase coded particles are used to construct phase plates to generate orbital angular momentum beams with different topological charges.

REFERENCES

[1] S. Teng, Q. Zhang, H. Wang, L. Liu, and H. Lv, "Conversion between polarization states based on a metasurface," *Photon. Res.*, vol. 7, no. 3, pp. 246–250, 2019.

[2] X. Luo, Z. Tan, C. Wang, and J. Cao, "A reflecting-type highly efficient terahertz cross-polarization converter based on metamaterials," *Chin. Opt. Lett.*, vol. 17, no. 9, 2019, Art. no. 093101.

[3] W. Liang, Z. Li, Y. Wang, W. Chen, and Z. Li, "All-angle optical switch based on the zero reflection effect of graphene–dielectric hyperbolic metamaterials," *Photon. Res.*, vol. 7, no. 3, pp. 318–324, 2019.

[4] Y. Cui, G. Zheng, M. Chen, Y. Zhang, Y. Yang, J. Tao, T. He, and Z. Li, "Reconfigurable continuous-zoom metalens in visible band," *Chin. Opt. Lett.*, vol. 17, no. 11, 2019, Art. no. 111603.

[5] T. Hou, Y. An, Q. Chang, P. Ma, J. Li, D. Zhi, L. Huang, R. Su, J. Wu, Y. Ma, and P. Zhou, "Deep-learning-based phase control method for tiled aperture coherent beam combining systems," *High Power Laser Sci. Eng.*, vol. 7, no. 4, p. e59, 2019.

[6] H. Chen, J. Wang, H. Ma, S. Qu, Z. Xu, A. Zhang, M. Yan, and Y. Li, "Ultra-wideband polarization conversion metasurfaces based on multiple plasmon resonances," *J. Appl. Phys.*, vol. 115, no. 15, Apr. 2014, Art. no. 154504.

[7] H. Wang, J. Zheng, Y. Fu, C. Wang, X. Huang, Z. Ye, and L. Qian, "Multichannel high extinction ratio polarized beam splitters based on metasurfaces," *Chin. Opt. Lett.*, vol. 17, no. 5, 2019, Art. no. 052303.

[8] X. Zang, Y. Zhu, C. Mao, W. Xu, H. Ding, J. Xie, Q. Cheng, L. Chen, Y. Peng, Q. Hu, M. Gu, and S. Zhuang, "Manipulating terahertz plasmonic vortex based on geometric and dynamic phase," *Adv. Opt. Mater.*, vol. 7, no. 3, Feb. 2019, Art. no. 1801328.

[9] N. C. Pégard and J. W. Fleischer, "Optimizing holographic data storage using a fractional Fourier transform," *Opt. Lett.*, vol. 36, no. 13, pp. 2551–2553, 2011.

[10] M. R. Akram, M. Q. Mehmood, X. Bai, R. Jin, M. Premaratne, and W. Zhu, "High efficiency ultrathin transmissive metasurfaces," *Adv. Opt. Mater.*, vol. 7, no. 11, Jun. 2019, Art. no. 1801628.

[11] M. R. Akram, G. Ding, K. Chen, Y. Feng, and W. Zhu, "Ultrathin single layer metasurfaces with Ultra-Wideband operation for both transmission and reflection," *Adv. Mater.*, vol. 32, no. 12, Mar. 2020, Art. no. 1907308.

[12] M. R. Akram, X. Bai, R. Jin, G. A. E. Vandenbosch, M. Premaratne, and W. Zhu, "Photon spin Hall effect-based ultra-thin transmissive metasurface for efficient generation of OAM waves," *IEEE Trans. Antennas Propag.*, vol. 67, no. 7, pp. 4650–4658, Jul. 2019.

[13] M. Huault, D. De Luis, J. I. Apiñaniz, M. De Marco, C. Salgado, N. Gordillo, C. Gutiérrez Neira, J. A. Pérez-Hernández, R. Fedosejevs, G. Gatti, L. Roso, and L. Volpe, "A 2D scintillator-based proton detector for high repetition rate experiments," *High Power Laser Sci. Eng.*, vol. 7, no. 4, p. 60, 2019.

[14] L. Koirala, C. Park, S. Lee, and D. Choi, "Angle tolerant transmissive color filters exploiting metasurface incorporating hydrogenated amorphous silicon nanopillars," *Chin. Opt. Lett.*, vol. 17, no. 8, 2019, Art. no. 082301.

[15] M. I. Shalaev, J. Sun, A. Tsukernik, A. Pandey, K. Nikolskiy, and N. M. Litchinitser, "High-efficiency all-dielectric metasurfaces for ultracompact beam manipulation in transmission mode," *Nano Lett.*, vol. 15, no. 9, pp. 6261–6266, Sep. 2015.

[16] A. Howes, W. Wang, I. Kravchenko, and J. Valentine, "Dynamic transmission control based on all-dielectric Huygens metasurfaces," *Optica*, vol. 5, no. 7, pp. 787–792, 2018.

[17] C. R. Devlin, M. Khorasaninejad, W. T. Chen, J. Oh, and F. Capasso, "Broadband high-efficiency dielectric metasurfaces for the visible spectrum," *Proc. Nat. Acad. Sci. USA*, vol. 113, no. 38, pp. 10473–10478, 2016.

[18] N. Yu and F. Capasso, "Flat optics with designer metasurfaces," *Nature Mater.*, vol. 13, no. 2, pp. 139–150, Feb. 2014.

[19] A. Arbabi and A. Faraon, "Fundamental limits of ultrathin metasurfaces," *Sci. Rep.*, vol. 7, p. 43722, Mar. 2017.

[20] A. Forouzmand, S. Tao, S. Jafar-Zanjani, J. Cheng, M. M. Salary, and H. Mosallaei, "Double split-loop resonators as building blocks of metasurfaces for light manipulation: Bending, focusing, and flat-top generation," *J. Opt. Soc. Amer. B, Opt. Phys.*, vol. 33, no. 7, p. 1411, Jul. 2016.

[21] D. Zhang, X. Yang, P. Su, J. Luo, H. Chen, J. Yuan, L. Li, "Design of single-layer high-efficiency transmitting phase-gradient metasurface and high gain antenna," *J. Phys. D, Appl. Phys.*, vol. 50, no. 49, 2017, Art. no. 495104.

[22] M. Tonouchi, "Cutting-edge terahertz technology," *Nature Photon.*, vol. 1, no. 2, pp. 97–105, Feb. 2007.

[23] C. Lan, H. Ma, M. Wang, Z. Gao, K. Liu, K. Bi, J. Zhou, and X. Xin, "Highly efficient active all-dielectric metasurfaces based on hybrid structures integrated with phase-change materials: From terahertz to optical ranges," *ACS Appl. Mater. Interfaces*, vol. 11, no. 15, pp. 14229–14238, Apr. 2019.

[24] S. Liu, A. Noor, L. L. Du, L. Zhang, Q. Xu, K. Luan, T. Q. Wang, Z. Tian, W. X. Tang, J. G. Han, W. L. Zhang, X. Y. Zhou, Q. Cheng, and T. J. Cui, "Anomalous refraction and nondiffractive bessel-beam generation of terahertz waves through transmission-type coding metasurfaces," *ACS Photon.*, vol. 3, no. 10, pp. 1968–1977, Oct. 2016.

[25] J. He, T. Dong, B. Chi, and Y. Zhang, "Metasurfaces for terahertz wavefront modulation: A review," *J. Infr., Millim., Terahertz Waves*, vol. 41, no. 6, pp. 607–631, 2020.

[26] R. T. Ako, A. Upadhyay, W. Withayachumnankul, M. Bhaskaran, and S. Sriram, "Dielectrics for terahertz metasurfaces: Material selection and fabrication techniques," *Adv. Opt. Mater.*, vol. 8, no. 3, Feb. 2020, Art. no. 1900750.

[27] D. Yang, C. Zhang, X. Li, and C. Lan, "InSb-enhanced thermally tunable terahertz silicon metasurfaces," *IEEE Access*, vol. 7, pp. 95087–95093, 2019.

[28] H. Zhang, X. Zhang, Q. Xu, C. Tian, Q. Wang, Y. Xu, Y. Li, J. Gu, Z. Tian, C. Ouyang, X. Zhang, C. Hu, J. Han, and W. Zhang, "High-efficiency dielectric metasurfaces for polarization-dependent terahertz wavefront manipulation," *Adv. Opt. Mater.*, vol. 6, no. 1, Jan. 2018, Art. no. 1700773.

[29] D. Jia, Y. Tian, W. Ma, X. Gong, J. Yu, G. Zhao, and X. Yu, "Transmissive terahertz metalens with full phase control based on a dielectric metasurface," *Opt. Lett.*, vol. 42, no. 21, p. 4494, Nov. 2017.

[30] Z. Ma, M. Stephen Hanham, P. Albella, B. Ng, H. T. Lu, Y. Gong, A. S. Maier, and M. Hong, "Terahertz all-dielectric magnetic mirror metasurfaces," *ACS Photon.*, vol. 3, no. 6, pp. 1010–1018, 2016.

[31] H. Cai, Q. Huang, X. Hu, Y. Liu, Z. Fu, Y. Zhao, H. He, and Y. Lu, "All-optical and ultrafast tuning of terahertz plasmonic metasurfaces," *Adv. Opt. Mater.*, vol. 6, no. 14, 2018, Art. no. 1800143.
[32] X. Bie, X. Jing, Z. Hong, and C. Li, "Flexible control of transmitting terahertz beams based on multilayer encoding metasurfaces," *Appl. Opt.*, vol. 57, no. 30, pp. 9070–9077, 2018.
[33] M. Pu, P. Chen, C. Wang, Y. Wang, Z. Zhao, C. Hu, C. Huang, and X. Luo, "Broadband anomalous reflection based on gradient low-Q meta-surface," *AIP Adv.*, vol. 3, May 2013, Art. no. 052136.
[34] T. J. Cui, M. Q. Qi, X. Wan, J. Zhao, and Q. Cheng, "Coding metamaterials, digital metamaterials and programmable metamaterials," *Light: Sci. Appl.*, vol. 3, no. 10, p. e218, Oct. 2014.
[35] M. Paquay, J.-C. Iriarte, I. Ederra, R. Gonzalo, and P. de Maagt, "Thin AMC structure for radar cross-section reduction," *IEEE Trans. Antennas Propag.*, vol. 55, no. 12, pp. 3630–3638, Dec. 2007.
[36] W. M. Lee, X.-C. Yuan, and W. C. Cheong, "Optical vortex beam shaping by use of highly efficient irregular spiral phase plates for optical micromanipulation," *Opt. Lett.*, vol. 29, no. 15, pp. 1796–1798, 2004.
[37] D. W. Zhang and X. C. Yuan, "Optical doughnut for optical tweezers," *Opt. Lett.*, vol. 28, no. 9, pp. 740–742, May 2003.
[38] A. E. Willner and Y. Fainman, "Optical communications using orbital angular momentum beams," *Adv. Opt. Photon.*, vol. 7, pp. 66–106, Mar. 2015.
[39] J. Liang and S. Zhang, "Orbital angular momentum (OAM) generation by cylinder dielectric resonator antenna for future wireless communications," *IEEE Access*, vol. 4, pp. 9570–9574, 2016.
[40] A. M. Yao and M. J. Padgett, "Orbital angular momentum: Origins, behavior and applications," *Adv. Opt. Photon.*, vol. 3, no. 3, pp. 161–204, Jun. 2011.
[41] D.-S. Ding, W. Zhang, and Z. Y. Zhou, "Quantum storage of orbital angular momentum entanglement in an atomic ensemble," *Phys. Rev. Lett.*, vol. 114, no. 5, 2015, Art. no. 050502.
[42] X. B. Zou and W. Mathis, "Scheme for optical implementation of orbital angular momentum beam splitter of a light beam and its application in quantum information processing," *Phys. Rev. A, Gen. Phys.*, vol. 71, no. 4, pp. 527–532, 2005.
[43] P. Wang, X. Zhang, and D. Fan, "Convolutional neural network-assisted optical orbital angular momentum recognition and communication," *IEEE Access*, vol. 7, pp. 162025–162035, 2019.
[44] J. Lin, X.-C. Yuan, M. Chen, and J. C. Dainty, "Application of orbital angular momentum to simultaneous determination of tilt and lateral displacement of a misaligned laser beam," *J. Opt. Soc. Amer. A, Opt. Image Sci.*, vol. 27, no. 10, pp. 2337–2343, Oct. 2010.
[45] V. Grillo, A. H. Tavabi, F. Venturi, H. Larocque, R. Balboni, G. C. Gazzadi, S. Frabboni, P.-H. Lu, E. Mafakheri, F. Bouchard, R. E. Dunin-Borkowski, R. W. Boyd, M. P. J. Lavery, M. J. Padgett, and E. Karimi, "Measuring the orbital angular momentum spectrum of an electron beam," *Nature Commun.*, vol. 8, no. 1, Aug. 2017.
[46] F. Bi, Z. Ba, and X. Wang, "Metasurface-based broadband orbital angular momentum generator in millimeter wave region," *Opt. Express*, vol. 26, no. 20, pp. 25693–25705, Oct. 2018.
[47] S. Jiang, C. Chen, H. Zhang, and W. Chen, "Achromatic electromagnetic metasurface for generating a vortex wave with orbital angular momentum (OAM)," *Opt. Express*, vol. 26, no. 5, pp. 6466–6477, 2018.
[48] M. R. Akram, G. Ding, K. Chen, Y. Feng, and W. Zhu, "Ultra-thin single layer metasurfaces with ultra-wideband operation for both transmission and reflection," *Adv. Mater.*, vol. 32, no. 12, Mar. 2020, Art. no. 1907308.
[49] Z. Lin, Z. Ba, and X. Wang, "Broadband high-efficiency electromagnetic orbital angular momentum beam generation based on a dielectric metasurface," *IEEE Photon. J.*, vol. 12, no. 3, pp. 1–11, Jun. 2020.
[50] Y. Ran, T. Cai, L. Shi, J. Wang, J. Liang, S. Wu, J. Li, and Y. Liu, "High-performance transmissive broadband vortex beam generator based on Pancharatnam–Berry metasurface," *IEEE Access*, vol. 8, pp. 111802–111810, 2020.
[51] H. Zhou, J. Dong, S. Yan, Y. Zhou, and X. Zhang, "Generation of terahertz vortices using metasurface with circular slits," *IEEE Photon. J.*, vol. 6, no. 6, pp. 1–7, Dec. 2014.
[52] H. Zhao, B. Quan, X. Wang, C. Gu, J. Li, and Y. Zhang, "Demonstration of orbital angular momentum multiplexing and demultiplexing based on a metasurface in the terahertz band," *ACS Photon.*, vol. 5, no. 5, pp. 1726–1732, May 2018.
[53] J. Fan and Y. Cheng, "Broadband high-efficiency cross-polarization conversion and multi-functional wavefront manipulation based on chiral structure metasurface for terahertz wave," *J. Phys. D, Appl. Phys.*, vol. 53, no. 2, Jan. 2020, Art. no. 025109.
[54] R. Dharmavarapu, K.-I. Izumi, I. Katayama, S. H. Ng, J. Vongsvivut, M. J. Tobin, A. Kuchmizhak, Y. Nishijima, S. Bhattacharya, and S. Juodkazis, "Dielectric cross-shaped-resonator-based metasurface for vortex beam generation at mid-IR and THz wavelengths," *Nanophotonics*, vol. 8, no. 7, pp. 1263–1270, Jul. 2019.
[55] X. Zang, Y. Zhu, C. Mao, W. Xu, H. Ding, J. Xie, Q. Cheng, L. Chen, Y. Peng, Q. Hu, M. Gu, and S. Zhuang, "Manipulating terahertz plasmonic vortex based on geometric and dynamic phase," *Adv. Opt. Mater.*, vol. 7, no. 3, Feb. 2019, Art. no. 1801328.
[56] Y. Yang, W. Wang, P. Moitra, I. I. Kravchenko, D. P. Briggs, and J. Valentine, "Dielectric meta-reflectarray for broadband linear polarization conversion and optical vortex generation," *Nano Lett.*, vol. 14, no. 3, pp. 1394–1399, Mar. 2014.
[57] M. Pu, X. Li, X. Ma, Y. Wang, Z. Zhao, C. Wang, C. Hu, P. Gao, C. Huang, H. Ren, X. Li, F. Qin, J. Yang, M. Gu, M. Hong, and X. Luo, "Catenary optics for achromatic generation of perfect optical angular momentum," *Sci. Adv.*, vol. 1, no. 9, Oct. 2015, Art. no. e1500396.
[58] X. Ding, F. Monticone, K. Zhang, L. Zhang, D. Gao, S. N. Burokur, A. de Lustrac, Q. Wu, C.-W. Qiu, and A. Alu, "Ultrathin pancharatnam-berry metasurface with maximal cross-polarization efficiency," *Adv. Mater.*, vol. 27, no. 7, pp. 1195–1200, Feb. 2015.
[59] F. Monticone, N. M. Estakhri, and A. Alu, "Full control of nanoscale optical transmission with a composite metascreen," *Phys. Rev. Lett.*, vol. 110, no. 20, May 2013.
[60] M. L. N. Chen, L. J. Jiang, and W. E. I. Sha, "Ultrathin complementary metasurface for orbital angular momentum generation at microwave frequencies," *IEEE Trans. Antennas Propag.*, vol. 65, no. 1, pp. 396–400, Jan. 2017.
[61] Q. Wei, L. Huang, T. Zentgraf, and Y. Wang, "Optical wavefront shaping based on functional metasurfaces," *Nanophotonics*, vol. 9, no. 5, pp. 987–1002, Feb. 2020.
[62] B. Fang, Y. Ke, L. Jiang, J. Cai, H. Gan, M. Zhang, C. Li, and Z. Hong, "Continuous scattering angle control of transmission terahertz wave by convolution manipulation of all-dielectric encoding metasurfaces," *Appl. Phys. A, Solids Surf.*, vol. 126, p. 619, 2020.
[63] S. Rubin and Y. Fainman, "Nonlinear, tunable, and active optical metasurface with liquid film," *Adv. Photon.*, vol. 1, no. 6, 2019, Art. no. 066003.
[64] A. Hanuka, K. P. Wootton, Z. Wu, K. Soong, I. V. Makasyuk, R. J. England, and L. Schächter, "Cumulative material damage from train of ultrafast infrared laser pulses," *High Power Laser Sci. Eng.*, vol. 7, no. 7, p. e7, 2019.

XUFENG JING received the degree and the Ph.D. degree from the Shanghai Institute of Optics and Fine Mechanics, Chinese Academy of Sciences (CAS), in 2011. He is an Associate Professor with the Institute of Optoelectronics Technology, China Jiliang University, and a master's tutor. His research interests include nano-photonics, metamaterials, and metasurfaces.

YOUHUANG KE is currently pursuing the master's degree with China Jiliang University.

YING TIAN received the degree and the Ph.D. degree from the Shanghai Institute of Optics and Fine Mechanics, Chinese Academy of Sciences (CAS), in 2012. She is an Associate Professor with the Institute of Optoelectronics Technology, China Jiliang University, and a master's tutor.

HAIYONG GAN is a Research Scientist with the National Institute of Metrology, China. His research interests include single-photon metrology, absolute cryogenic radiometer, radiometric measurement standard and technology, and the spectroscopic characterization of advanced optical materials. He is currently the Chairperson of the Technical Committee of Photometry and Radiometry of the Asia Pacific Metrology Programme.

YINGWEI HE is an Associate Professor with the National Institute of Metrology, Beijing, China. His research interests include single-photon measurement and weak light emission standard technology.

CHENXIA LI is an Associate Professor with the Institute of Optoelectronics Technology, China Jiliang University, and a master's tutor.

ZHI HONG received the bachelor's and master's degrees from the Department of Electrical Engineering, Zhejiang University, in 1984 and 1987, respectively, and the Ph.D. degree in optical engineering from Zhejiang University in 2001. From 1987 to 2005, he was a Researcher and a Doctoral Tutor with the Department of Optics, Zhejiang University. He was with the Centre for THz Research, China Jiliang University. From 1999 and 2000, he went to work twice at Berkeley, Germany. He was a Visiting Professor with the University of Alberta, Canada, in 2006, and the Center for Terahertz Research, Rensselaer Institute of Technology, in 2007. He is a Research Fellow of the China Institute of Mechatronics Engineering.